Investigation of Swirling and Tumbling Flow Pattern of Spark Ignition Engine

O. Samimi Abianeh*
MSc. Student
Mechanical Engineering Department
Tarbiat Modares University
Tehran, Iran
o_samimi@ip-co.com

* Corresponding Author
Received: Sep. 10, 2007
Accepted in revised form: Apr. 21, 2009

M. Mirsalim
Assistant Professor
Mechanical Engineering Department
Amirkabir University
Tehran, Iran
mo_mirsalim@yahoo.com

A. Shafiei Sabet
Iran Khodro Engine Research Center (IPCO)
A_Shafiei@ip-co.com

Abstract

Gas motion within the cylinder is one of the major factors that control the combustion process in spark ignition engine. It also has significant impact on heat transfer. Both the bulk gas motion and the turbulence characteristics of the flow are important and governing the overall behavior of the flow. An arrangement for obtaining a stratified charge, using port injection, is proposed for a current design of a spark ignition engine. The behavior of combustion are simulated with Computational fluid dynamic and tested. Engine testing was performed using dynamometer for measuring the lean burn limit of the current spark ignition engine. Some concepts for premixed lean burn are introduced during the previous decade and with this state of the art concept the swirl and tumble flow pattern can generate in each speed, therefore the effect of these pattern on lean burn limit is investigated.

Keywords: Swirl Flow Pattern, Tumble FlowPattern, Lean Burn, Brake Specific Fuel Consumption, Brake Mean Effective Pressure

1. Introduction

Charge stratification is an effective measure to extend lean burn or EGR limits in spark ignition engines and therefore gives an increased fuel economy and decreased NO_X and CO_2 emissions. It can be achieved by means of strong large-scale air flow (swirl, tumble or inclined-axis swirl), but different company use different flow pattern to achieve more stable combustion for example: Mitsubishi [1 and 2] and Subaru adopt tumble as the large scale eddy to preserve the energy. Honda [3] adopts swirl, and Toyota [4 and 5], Nissan [6] and Mazda [7] adopt so-called inclined swirl, that is the flow combined tumble and swirl.

For investigation the flow pattern three models are tested, base line-engine, port with flow control baffle No. 1 (block

half of the port entrance, see fig. 1) and finally port with flow control baffle No. 2 (block the entire one intake valve, see fig. 1).

With the first flow control baffle, the part of the intake port entrance is blocked so the flow during entering the cylinder rotates and produces different bulk motion, swirl (Fig. 1), and with another flow control baffle the entire of one of the intake valve (from two intake valves) is covered (Fig. 1).

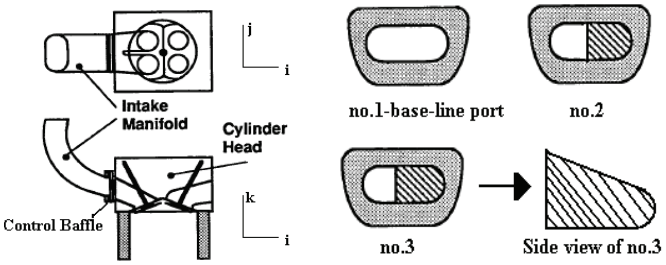

Fig. 1. Flow control baffles

The experimental tests and engine simulation were done at an engine operating condition of 2000 rev/min, 2 bar Brake mean effective pressure (BMEP). Motored tests are conducted on a four valves, four cylinders engine with geometric characteristics summarized in table 1.

TABLE 1. Engine specification

Fuel type	Gasoline
Bore × Stroke (mm×mm)	83 × 72
Displacement (cm^3)	1400
Bore (mm)	78.6
Compression ratio	10.5
IVO/IVC	39 °BTDC/ 64 °ABDC
EVO/EVC	17 °BBDC/ 9 °ATDC

2. Experimental Procedure

Swirl and tumble ratios are usually measured in a steady flow rig for a given valve lift. A torque meter is used to quantify the charge motion torque. To measure swirl, the torque meter is mounted at the bottom of the cylinder. The air flow is sucked up through the inlet port, to simulate the operation of a naturally aspirate engine. Unlike swirl, the generation of tumbling motion is not only outflow characteristics of the intake system but also the impinging on the piston. Thus the specific design is required to take into account the piston effect. The tumble ratio values so determined are specific of the design of the tumble rig and cannot be directly compared to data obtained from other tumble rigs (Fig. 2). For the steady state flow rig, the swirl ratio and tumble ratio are defined as below:

$$C_s = \frac{8T}{\dot{m} v_\circ B} \tag{1}$$

where T is the torque and is the air mass flow rate and the bore (B) has been used as characteristic dimension. The velocity is defined by:

$$v_\circ = \left(2\frac{P_\circ - P}{\rho}\right)^{0.5} \tag{2}$$

$(P_\circ - P)$ is the pressure drop across the valve using an incompressible flow equation. For the CFD calculation, the swirl ratio Rs (and Tumble ratio Rt) is defined as the ratio of the angular velocity of in-cylinder flow to the engine angular velocity N:

$$R_s = \omega / N \tag{3}$$

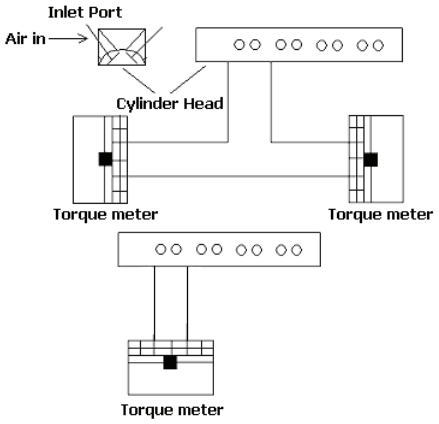

Fig. 2. Steady flow rig, tumble meter apparatus (Top) and swirl meter (bottom)

Fig. 3. Steady flow rig, swirl meter (right), Tumble meter (left)

The relationship between steady-flow rig tests (which are extensively used because of their simplicity) and actual engine swirl patterns is not fully understood. Steady flow tests adequately describe the swirl generating characteristics of the intake port and valve (at fixed valve lift) and are used extensively for this purpose. However, the swirling flow set up in cylinder during intake can change significantly during compression [8].

The device that is shown figure 4 is used to measure the injector parameters.

The sprayed quantity is collected and measured separately for each of the 8 segments in a measuring insert shown in fig. 4.

The results of the test for calibration the injector model is shown in table 2.

TABLE 2. Injector specification

	S	X	Y	Z	D	Q(stat)	Q(dyn)
α	mm	mm	mm	mm	mm	g/min	g/1000
15	28	7	17.6	36.4	100	158.2	4.8

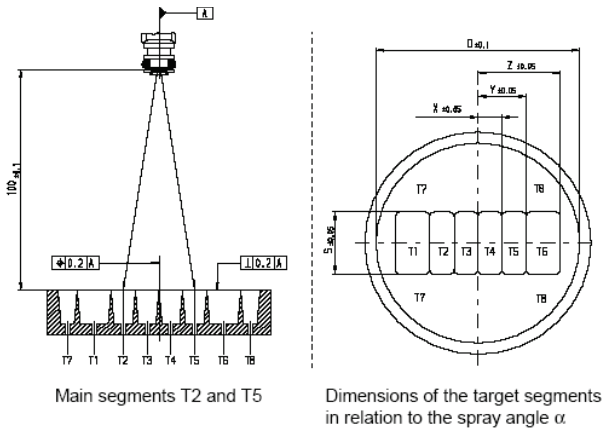

Main segments T2 and T5

Dimensions of the target segments in relation to the spray angle α

Fig. 4. Injector flow measurement

3. CFD modeling

All CFD calculations were performed using VECTIS[1]. The code is characterized by the feature of automatic generation of computational grid based on the cut cell technique for wall surfaces. Due to the fact that it is automatic, the labour required for mesh generation is relatively low and the method can be incorporated into the flow of the engine development cycle that usually has strict time constraints.

Fundamental equations are first discretised using the finite volume method, and then solved fully-implicitly, with coupling between variables and non-linear effects incorporated using iterative or predictor corrector methods. Transient or steady flows can be calculated.

The effect of turbulence is represented by the k-ε model. In the k-ε model, the molecular diffusivity for each transported variable is augmented by a turbulent diffusivity calculated from the turbulent kinetic energy (k) and its dissipation rate (ε), for which additional transport equations are solved. To avoid degeneracy problems, The PISO algorithm is used to couple the pressure and velocity for both compressible and incompressible flows.

The initial conditions insides the cylinder was assumed to be an inert gas with the cylinder pressure and temperature at intake TDC. The boundary conditions with and without flow control baffles are extracted from experimental tests.

The 2-phase spray model accounts for full interaction between the gas and liquid phases.

Fuel sprays are treated as a dispersed liquid phase, which moves in and interacts with the surrounding continuous gas phase. A fuel spray is represented by an ensemble of discrete droplet "parcels", each parcel containing a number of droplets with the same size, velocity and temperature. The droplet parcels are tracked in a Lagrangian fashion as they move through the gas phase, exchanging mass, momentum and energy. The affect of the droplet parcels on the continuous phase due to drag, heat and mass transfer is implemented via source terms in the gas phase conservation equations.

Sub models are provided for droplet break up, coalescence, turbulence interaction, wall impingement and re-entrainment.

1- CFD package from Ricardo Company

The momentum equation for a droplet of mass md is described by Newton's Law:

$$m_d \frac{dU_d}{dt} = \frac{1}{2} C_d \rho A_d \left| U - U_d (U - U_d) \right| \tag{4}$$

where C_d is the drop drag coefficient, ρ is the gas density and A_d is the drop frontal area.
The drag force depends on the relative velocity between ambient and drop:

$$U_r = U - U_d \tag{5}$$

The drag coefficient suggested by Putnam [9] is used for the trajectory calculation:

$$C_d = \begin{Bmatrix} \mathrm{Re}_d \le 1000: \\ \dfrac{24}{\mathrm{Re}_d}\left(1 + \dfrac{1}{6}\mathrm{Re}_d^{\frac{2}{3}}\right) \\ \mathrm{Re}_d \ge 1000: \\ 0.424 \end{Bmatrix} \tag{6}$$

The drop Reynolds number is defined as:

$$\mathrm{Re}_d = \left(\rho U_r D_r\right)/\mu \tag{7}$$

where μ is the gas dynamic viscosity. This empirical formula is suitable for numerical integration and has demonstrated reasonably accuracy against experimental data. When Reynolds numbers tend to zero, the formula becomes the Stokes Law, i.e.

$$C_d = 24/\mathrm{Re}_d \tag{8}$$

For high Reynolds numbers, the drag coefficient approaches a stable value.

The evaporation of drops in a spray involves simultaneous heat and mass transfer processes. The heat for evaporation is transferred to the drop surface by convection and conduction from the surrounding gas, the vapour is transferred back to the gas stream by convection and diffusion. The droplet mass and temperature are calculated from the Eqs. [10] and [11] as below:

$$\frac{dm_d}{dt} = -A_d \, Sh \frac{D_{AB}}{D_d} \rho_v \ln\left(\frac{P - P_{v,\infty}}{P - P_{v,s}}\right) \tag{9}$$

$$m_d \frac{dC_{p,d} T_d}{dt} = -A_d \, Nu \, (T_d - T) K_m F_z + h_{fg} \frac{dm_d}{dt}$$

where D_{AB} is the mass diffusivity, K_m is the mixture thermal conductivity, $C_{p,d}$, is the specific heat of liquid fuel, h_{fg} is the latent heat of evaporation, p is the pressure of gas mixture, and $P_{v,s}$, and $P_{v,\infty}$ stand for the partial pressure at the drop surface and ambient, respectively.

The fuel vapour density ρ_v is evaluated from the gas pressure and mean temperature,

$$T_m = (T_d + T)/2 \tag{10}$$

The Sherwood and Nusselt numbers, Sh and Nu, are calculated by the correlation by Ranz and Marshall [12]:

$$Sh = 2\left(1 + 0.3\,\mathrm{Re}_d^{\frac{1}{2}}\,Sc^{\frac{1}{3}}\right)$$
$$Nu = 2\left(1 + 0.3\,\mathrm{Re}_d^{\frac{1}{2}}\,\mathrm{Pr}^{\frac{1}{3}}\right) \tag{11}$$

A gasoline atomization model developed at the Engine Research Centre of Wisconsin University [13 to predict the atomization conditions of gasoline injectors with reasonable accuracy. This model contains two elements: the first is concerned with estimating the initial thickness and velocity of the liquid sheet at the orifice exit and the sheet breakup length, given that the injection pressure, injection mass flow rate, and orifice diameter are known; the second involves representing the continuous sheet as a number of discrete blobs and evaluating their primary breakup processes using the TAB (Taylor-Analogy Breakup) breakup model [14].

The model of Gosman and Bai is used to model the injector behaviour for different regimes of wall roughness, fuel and wall temperature, impingement angle and speed etc.

As the liquid phase is numerically modelled using the Lagrangian approach, injection of continuous conical liquid sheet at the injector is effected by introducing a number of blobs, or parent droplet parcels, at each computational time step, each with a diameter equal to the initial sheet thickness and velocity respectively, at the corresponding injection time. Each blob has a lifetime equal to its breakup time during which it experiences no air drag and has no interaction with other blobs or droplets. The atomization of each blob is calculated according to the TAB model. In this, an oscillating and distorting droplet is viewed as a mass-spring system, in which the external force acting on the mass, the restoring force of the spring and the damping force are taken in an analogous way as aerodynamic force exerted on the droplet, surface tension force and droplet viscous force respectively. Thus, a forced and harmonic oscillation of the droplet is described by the following equation:

$$\frac{d^2y}{dt^2} + \frac{5\mu_l}{\rho_l r_b^2}\frac{dy}{dt} + \frac{8\sigma}{\rho_l r_b^3} - \frac{2}{3}\frac{\rho_g U^2}{\rho_l r_b^3} = 0 \tag{12}$$

where y is droplet oscillation parameter scaled with the blob radius r_b , ρ_b and is the ambient gas density. The criterion for droplet breakup is $y \rangle 1$. Once this condition is reached, the droplet starts to disintegrate into a collection of small droplets which are assumed to observe Rosin-Rammler distribution described by:

$$f(D) = \frac{q\,D^{q-1}}{\overline{D}^q}\exp\left[-\left(\frac{D}{\overline{D}}\right)^q\right] \tag{13}$$

Where $\overline{D}$ is related to the Sauter mean diameter D_{32} as:

$$\overline{D} = D_{32}\,\Gamma\left(1 - \frac{1}{q}\right) \tag{14}$$

To evaluate D_{32} , energy balance before and after breakup is invoked to give:

$$D_{32} = 2r_b\left[\frac{7}{3} + \frac{\rho_l r_b^3 (dy/dt)^2}{8\sigma}\right]^{-1} \tag{15}$$

For fuel droplet impingement, liquid which sticks to the wall becomes a film. Heat and mass transfer of the wall film is calculated, so that fuel which impinges on the wall can evaporate from the wall and rejoin the calculation. Models that are used in this study are listed in table 3.

TABLE 3. Simulation characteristics

	Models
Gasoline Atomization	ERC
Droplet Break up	TAB (Taylor Analogy Break up)
Wall roughness	Gosman and Bai
Sherwood and Nusselt Number	Ranz and Marshal

4. Results and discussions

Tumble ratio curves measured on the steady flow bench are presented in fig. 3 as a function of valve lift, for the various flow control baffles. For the base line-engine configuration without baffle between cylinder head and intake manifold, no significant swirling motion is induced. (Fig. 4)

For base line engine, two bulk swirl are generated but in opposite direction as the result of port shape. Because of this matter the swirl meter test rig shows the zero torque for swirling motion (as we expected for engine with two similar intake valves). Tumble ratio that is measured in the steady flow rig is shown in Figs. 5 and 6.

For base line engine two swirling motion are generated in opposite direction therefore no significant swirling motion is induced and measured in Swirl meter.

Fig. 6 shows the evolution of swirl ratio in function of the valve lift for different flow control baffles.

Tumble ratio of three configurations is the same but swirl ration differ a lot between configurations.

By using CFD calculation the trend of Tumbling motion and swirling motion versus crank angle is investigated

Swirl ratio measured by CFD calculation is presented in Fig. 7.

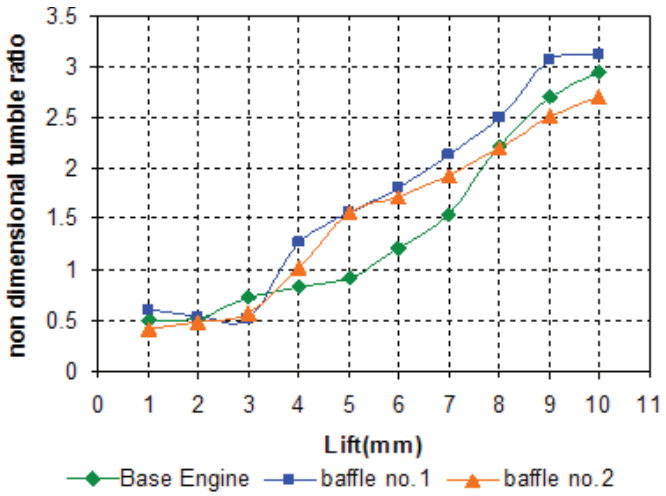

Fig. 5. Tumble ratio with various flow-controls baffles designs

Fig. 4 shows the evolution of swirl ratio in function of the valve lift for different flow control baffles.

From Fig. 7, it is observed that the swirling motion of flow control baffle Nos. 1 and 2 is existed up to the end of compression stroke. In base line engine, two opposite swirl is generated that canceled each other in the total volume of the cylinder (fig. 8). In all the figs. 0 is TDC of gas exchange. It is notable that the swirl ratio based on the steady state test rig for baffle No.2 is higher than baffle No.1 (fig. 4) but as shown in fig. 7 this matter is not true completely. [8]

Tumble ratio in two other axes is presented in Figs 9 and 10. The tumble ratio of both control baffles is higher than base line engine and the behaviors of tumble ratio in both axes of control baffles are the same.

In this paper the total rotation ratio is defined as:

$$\text{Rotation ratio} = Rs_i^2 + Rs_j^2 + Rs_k^2 \qquad (16)$$

The rotation ratio is presented in fig. 9. The rotation ratio of flow control baffle No.1 is higher than the control baffle No. 2. The rotation ratio of two control baffles is higher than the base-line engine.

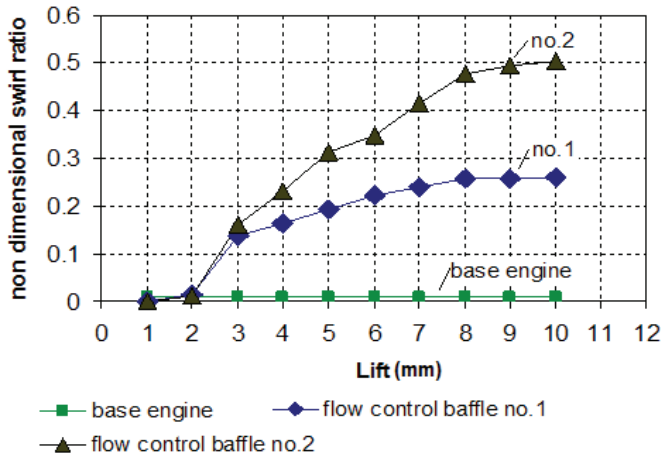

Fig. 6. Swirl ratio with various flow-controls baffles designs

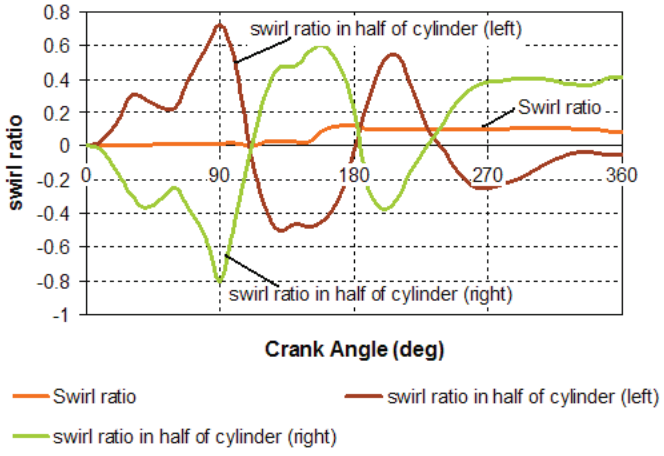

Fig. 8. Swirl ratio in base line engine based on CFD calculation (left side of cylinder and right side).

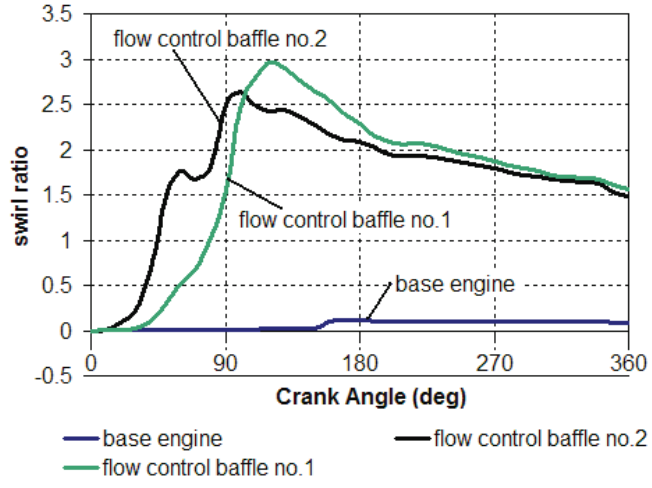

Fig. 7. Comparison of swirl ratio (Rs) between various control baffles by using of CFD calculation

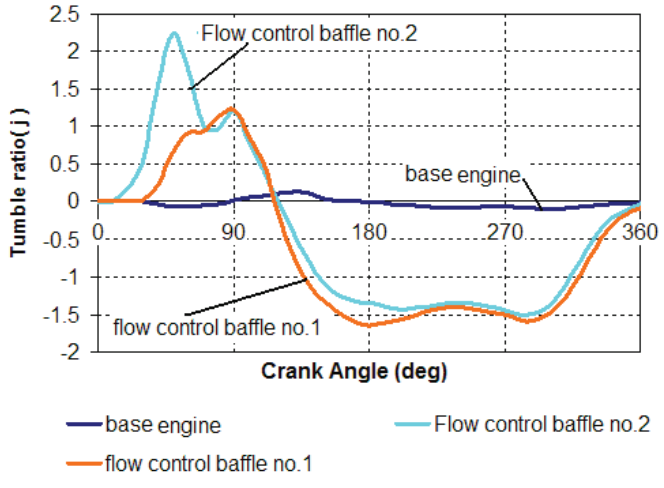

Fig. 9. Comparison of tumble (j axis) ratio between various control baffles by using of CFD calculation.

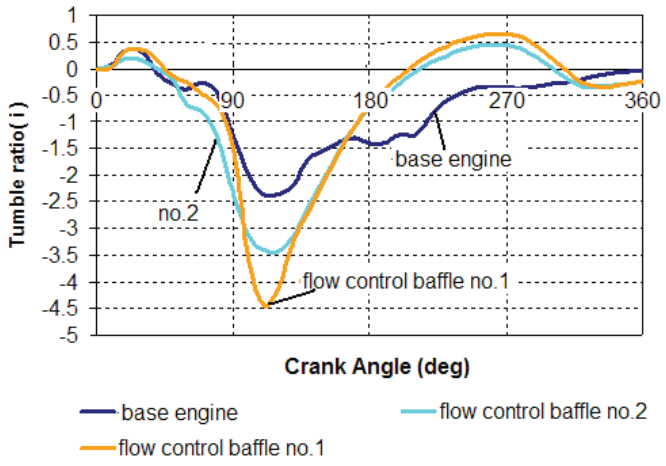

Fig. 10. Comparison of tumble (i axis) ratio between various control baffles by using of CFD calculation.

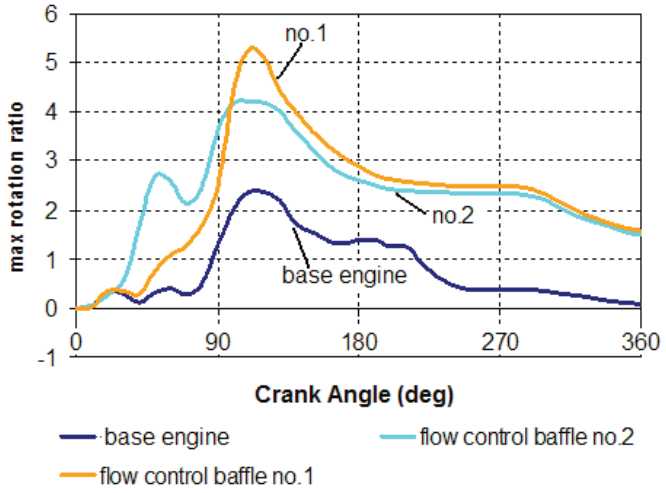

Fig. 11. Comparison of rotation ratio between various control baffles by using of CFD calculation.

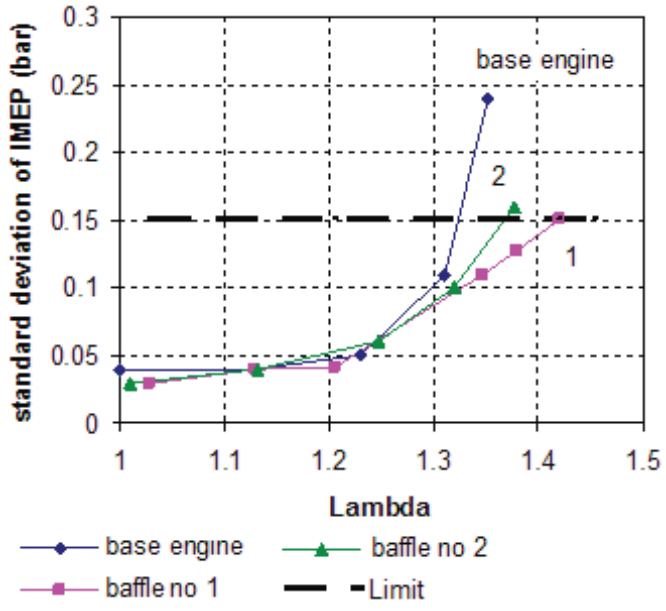

Fig. 12. COV of IMEP of cylinder, for base line-engine: Cylinder No. 4, for flow control baffles Nos. 1 and 2: cylinder No. 2.

5. Experimental results

Lean Burn limit can be judged from the relations of coefficient of variation (COV) in indicated mean effective pressure (IMEP) versus air/fuel ratio at part load condition. For base line engine, the maximum COV of IMEP occurs in cylinder No. 4 and for flow control baffles Nos. 1 and 2, it occurs in cylinder No. 4. Because of various flow fields and different temperature of cylinders, the COV of IMEP of cylinders is not the same, the maximum COV of IMEP is occurred in cylinder number as shown in table 3 and Fig. 12.

TABLE 4. Cylinder number of maximum of standard deviation of IMEP (numbering from flywheel side)

Name	Cylinder number	Lambda
Base line-engine	4	1.33
Flow control baffle No.1	2	1.49
Flow control baffle No.2	2	1.42

CO emissions are essentially insensitive to changes in ignition timing, as they are almost entirely a function of the A/f ratio. As observed in Fig. 13, The CO emission is not affected in mixture leaner than 1.2.

Although HC emissions mimic CO emissions by falling in response to higher excess air factors in the rich range, the hydrocarbon starts to rise in the lean range. Minimum HC emissions within the lean range occur at roughly lambda = 1.1 … 1.2.

The HC emissions for different control baffles are observed in Fig. 13. The HC emissions of engine with control baffle are higher than base line engine. This matter maybe occurs because of more heat transfer to the engine wall (due to higher rotation) and deeper quench zone that arises from lower combustion chamber temperature.

The relationship between NO_x and the excess-air factor (Lambda) is the reverse of the pattern described about HC. In the rich range, NO_x emissions respond to higher excess factors and their higher oxygen concentrations by climbing. In the lean range, NO_x emissions react to increases in excess air factor by falling, as the progressive reduction in mixture densities results in lower combustion-chamber temperatures.

Maximum NO_x emissions are encountered with moderate excess air in the lambda 1.05 to 1.1 ranges.

6. Injection results

The air/fuel ratio distribution for baffle No. 1 is smoother than other configuration and baffle No. 1 has a richest area around the spark (Fig. 16).

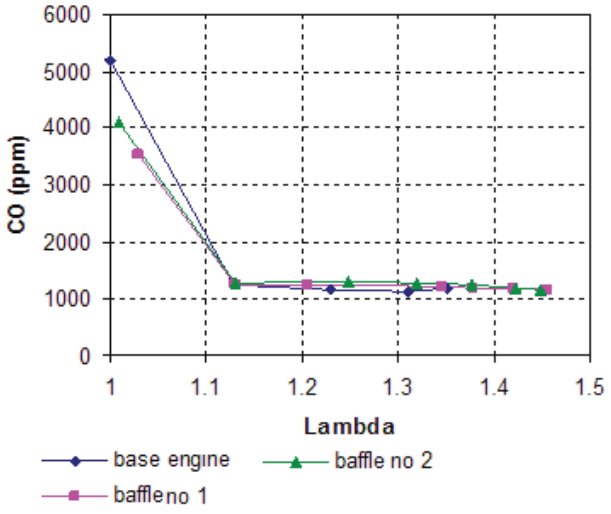

Fig.13. Effect of excess-air factor on CO emission for different configurations.

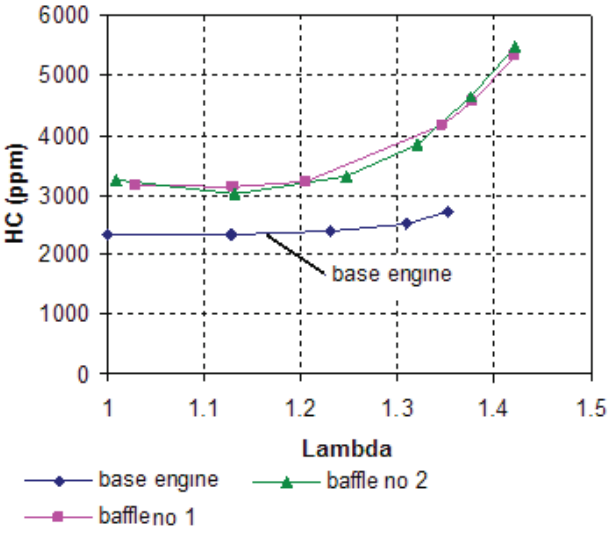

Fig. 14. Effect of excess-air factor on HC emissions for different configuration.

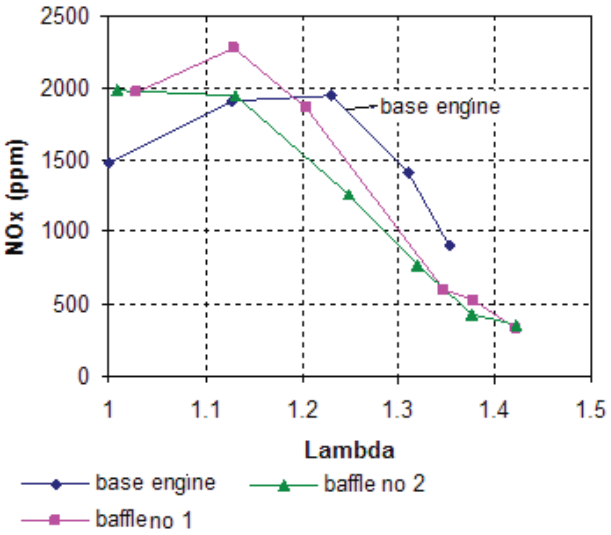

Fig.15. Effect of excess-air factor on NO_x emissions for different configuration.

The NO_x emission for engine with flow control baffle is 246 ppm in $\lambda = 1.49$ but it is 912 ppm for standard engine in $\lambda = 1.35$.

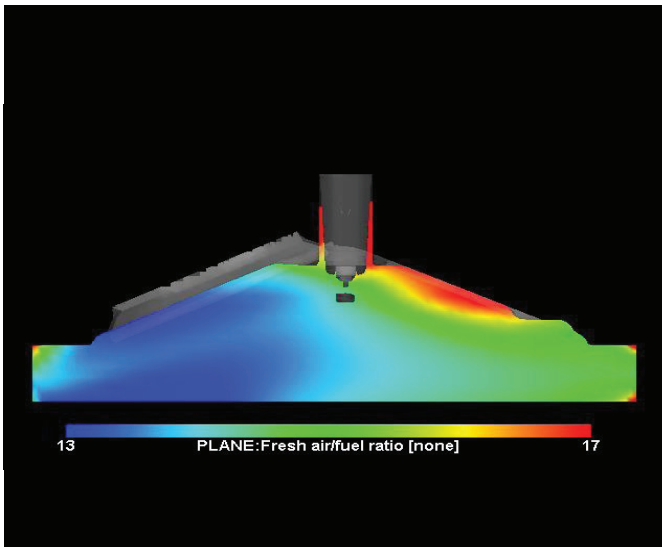

Fig. 16. Air/fuel ratio for baseline engine (330º CA)

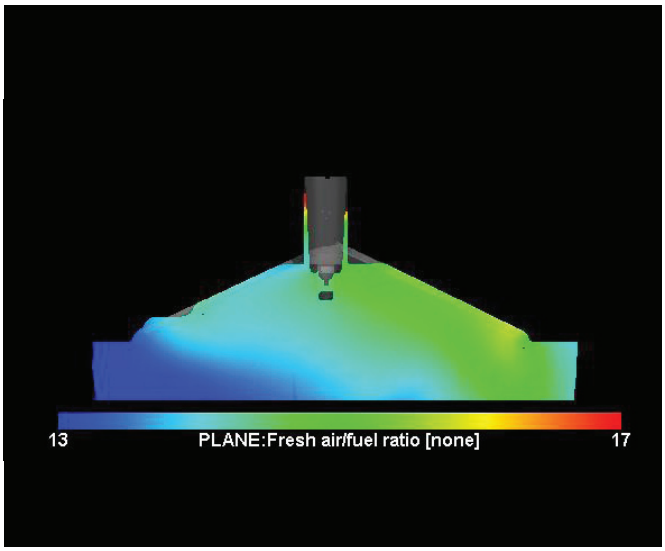

Fig. 17. Air/fuel ratio for baffle no.1 (330º CA)

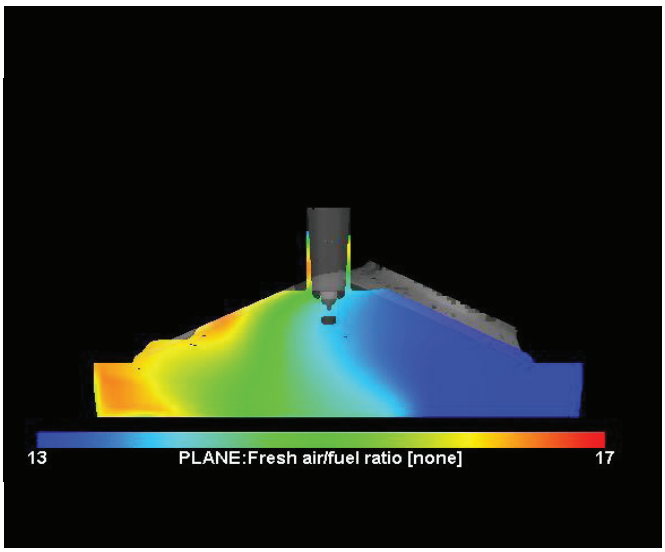

Fig. 18. Air/fuel ratio for baffle no.2 (330º CA)

7. Injection timing

The consequences of injection timing in terms of cylinder pressures are shown in figs. 19 and 20. It is clear that there is a minimum in the maximum pressure and mean-effective pressures

With the beginning of fuel injection at 300 ºCAD to 360 ºCAD and 420 ºCAD after top-dead-centre of intake and this corresponds to a maximum in the concentration of unburned hydrocarbons as would be expected. The variance of the mean-effective pressure is also a maximum at 360 ºCAD after intake and corresponds to a reduction in drivability. With injection over a wide range of crank angles corresponding to closed valves, there is little difference in the performance.

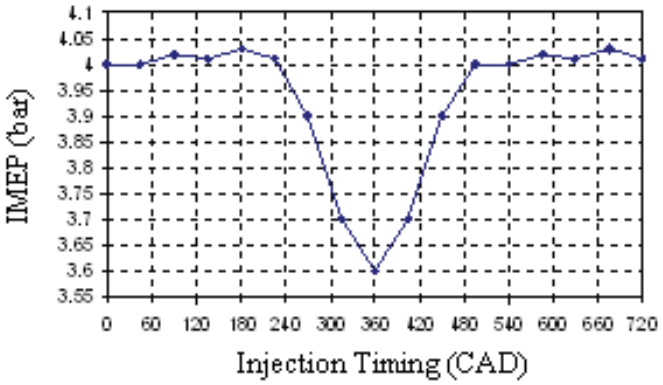

Fig. 19. Effect of injection timing on IMEP, 2000 rpm, and 90 ºC coolant temperature. (360 ºCAD TDC intake)

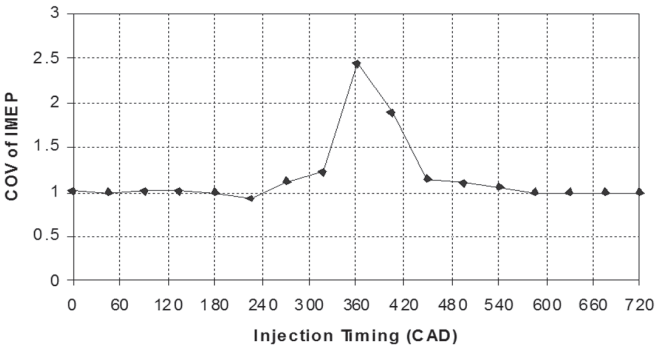

Fig. 20. Effect of injection timing on COV of IMEP, 2000 rpm, and 90 ºC coolant temperatures. (360 ºCAD ≡ TDC intake)

8. Conclusions

This study demonstrates the ability of an inlet system using flow-control baffle to induce swirling and tumbling motions in the four valve engine and to investigate the influence of swirling and tumbling motions in increasing the lean-limit of combustion.

CFD calculation and Flow Bench test rig show that the flow control baffle can change the flow pattern significantly.

Swirling motion can exist until the end of compression cycle but tumble motion is diminished faster, moreover, specific design of flow-control allows evaluating and comparing the potential of different inlet systems concerning engine combustion characteristics.

It is demonstrated the ability of swirling motion to improve engine stability compared to tumbling motion in current engine.

The engine with higher range of rotation ratio has better lean burn capability and this matter is the results of two opposite subjects, negative effect of more heat transfer and positive effects of more turbulence and orderly bulk flow.

The HC emissions of engine with higher flow rotation (swirl or tumble) is higher, because of thicker quench layer, higher heat transfer and larger fuel wet area.

In mass production, the flow control baffle can be replaced with control devices such as swirl control valve or valve deactivation mechanism that can be fully open in full load ■

REFRENCES:

1. Kiyota, Y., Akishino, K. and Ando, H., "Concept of Lean Burn Combustion by Barrel–Stratification", SAE Papers, No. 920678, 1992.
2. Kuwahara, K., Watanabe, T., Takemura, J., Omori, S., Kume, T. and Ando, H., "Optimization of In-cylinder Flow and Mixing for a Center-Spark Four Valve Engine Employing the Concept of Barrel", Stratification, SAE Papers, No. 940986, 1994.
3. Horie, K., Nishizawa, K., Ogawa, T., Akazaki, S. and Miura, K., "The Development of a High Fuel Economy and High Performance Four Valve Lean Burn Engine", SAE Papers, No. 920455, 1992.
4. Okano, H., Fukuma, T., Okumura, T. and Tkagi, N., Development of a Lean Burn Engine, 1991 JSAE Spring Convection, Japan, 1991, p.135.
5. Harada, J., Matushita, S., Okano, H., Nomura, T. and Okumura, T., Development of a New Generation Lean Burn Engine, 1992 JSAE Autumn Convection, Japan, 1992, No. 924, Vol. 2, p.69 (JSAE).
6. Saito, K. and Matsumura, M., Technologies for Reducing the Fuel Consumption of a New 1.5 Liter Engine (in Japanese), 1994 JSAE Spring Convection, Japan, 1994, No. 943, p. 5.
7. Mitobe, N., Fujimoto, M., Fujikawa, T., Shimizu, I., Honda, Y. and Nagao, A., *Technologies of a New 1.5 liter Burn Engine*, 1994, No. 944, p. 25 (JSAE).
8. Heywood. John B., *Internal Combustion Engine Fundamentals*, New York: MacGraw-Hill Book Company, 1988.
9. Putnam, A., "Integratable Form of Droplet Drag Coefficient", *J. Am. Rocket Soc.*, Vol. 31, (1961): 1467-1468.
10. Spalding, D. B., "The Combustion of Liquid Fuels", Fourth Symposium (International) on Combustion, Williams and Wilkins, Baltimore, (1953): 847-864.
11. Chin, J. S. and Lefebvre, A. H., "The Role of the Heat-up Period in Fuel Drop Evaporation", *Int. J. Turbo Jet Engines*, Vol. 2, (1985): 315-325.
12. Ranz, W. E. and Marshall, W. R., "Evaporation from Drops", Chem. Eng. Prog., Vol. 48, (1952) Part I, 141-146, Part II, 173-180.
13. Han, Z., Parrish, S., Farrell, P. V., and Reitz, R. D. Modeling Atomization Processes of Pressure Swirl Hollow-Cone Fuel Sprays, Vol. 7, (1997) 663-684.
14. O'Rourke, P. J. and Amsden, A., "The TAB Method for Numerical Calculation for Spray Droplet Breakup", SAE Papers, No. 872089, 1987.